Iranian Hydraulic Association
Journal of Hydraulics

Research Article
https://doi.org

The Controlling Role of Worst-Case Log Placement, Wood Characteristics, and Pier–Abutment Distance in Large Wood Accumulation Probability: A Laboratory Study

Saba Soori[1]*, Hojat Karami[2]

1- PhD Graduated, Department of Civil Engineering, Semnan University, Semnan, Iran.

2- Associate Professor, Department of Civil Engineering, Semnan University, Semnan, Iran.

*** soori.saba@semnan.ac.ir**

Abstract

The accumulation of large wood (LW) at bridge structures poses a significant flood hazard, yet the critical role of initial log placement in triggering these blockages remains insufficiently quantified. This study provides a systematic experimental investigation into the parameters governing the accumulation probability (AP) at bridge piers and abutments. It focuses on four key domains: (1) initial log placement conditions (release distance, lateral position, and orientation); (2) approach flow conditions; (3) geometric characteristics of the bridge, particularly the varying distance between the pier and abutment; and (4) LW characteristics, including length, diameter, branching, and transport regime (uncongested vs. congested). Results identified the worst-case scenario for LW accumulation around piers and abutments: logs released 1m upstream of the abutment nose, from the channel centerline, and oriented perpendicular to the flow. Furthermore, the analysis reveals that accumulation probability is predominantly a function of approach flow velocity, log length and diameter, and the distance between the pier and abutment. Overall, these findings provide a quantitative, design-oriented basis for estimating LW accumulation risk and for guiding the layout of pier–abutment systems to enhance resilience against wood-laden floods.

Keywords: Pier–abutment system; Large wood (LW); Accumulation probability (AP); Worst-case log placement; Bridge clogging; Log release conditions.

1. Introduction

Large wood (LW) can be defined as logs longer than 1 m and thicker than 0.1 m (Keller and Swanson, 1979). At bridges, LW accumulation increases backwater, hydrodynamic loading, and local scour, thereby elevating the risk of structural failure (Diehl, 1997, Lagasse, 2010, Schalko et al., 2020, Soori and Karami, 2025). At the same time, LW is a key ecological element that shapes river morphology and supports habitat and biodiversity (Gurnell et al., 2002, Wohl et al., 2016). During flood events, LW mobility can turn into a major infrastructure hazard, and severe impacts have been reported worldwide, from catastrophic floods in Central Europe (Schalko, 2018) to recent Iranian events culminating in bridge failures such as the Amir Deh Bridge collapse in 2022. Figure 1 provides a visual representation of the geographical location of the Amir Deh Bridge on the Sajjadrud River and its subsequent collapse. These cases highlight the need for improved LW–structure interaction models to support resilient design. Moreover, while Natural Flood Management can attenuate peak flows, it does not reliably reduce total flood volume (Bagheri-Gavkosh et al., 2025), reinforcing the importance of robust structural measures against wood-laden floods.

This finding underscores the need for resilient structural design against direct flood impacts, including hazards posed by LW accumulation. Often initiated by a large "key member," LW accumulations can rapidly develop into jams that increase flow resistance, raise upstream flood stages, and ultimately threaten structural stability (Diehl, 1997, Bradley et al., 2005, Panici and de Almeida, 2018, Panici and de Almeida, 2020, Soori and Karami, 2025). Nevertheless, the hydrodynamics controlling LW accumulation at complex bridge geometries remain insufficiently quantified, leaving a critical gap for design applications and risk assessment.

To establish a foundation for understanding this problem, it is essential to consider the fundamentals of wood transport during floods, as they strongly control how LW interacts with obstacles. Building on the framework of (Braudrick et al., 1997), three transport regimes can be distinguished from flume experiments: uncongested (logs move mainly as individual elements with limited interaction), semi-congested (intermediate interactions), and congested (bulk movement of wood). Extending this classification to field conditions, Ruiz-Villanueva et al. (2019) introduced hypercongested wood-laden flows, characterized by such high LW concentrations that the solid phase may rival or even exceed the liquid phase.

A substantial body of experimental research has therefore focused on LW accumulation probability at individual bridge elements. For instance, studies on bridge decks have demonstrated that the likelihood of clogging is highly sensitive to deck type (e.g., railing, truss, baffle), approach flow conditions (Froude number), and deck clearance (freeboard). Railing and truss bridges generally present the highest blockage risk, with probability decreasing as flow velocity increases (Bezzola and Hegg, 2007, Schmocker and Hager, 2011). Similarly, research on single piers of various shapes (e.g., cylindrical, rectangular, triangular) has identified log length, approach flow velocity, and the presence of roots or branches as key factors controlling accumulation probability(Gschnitzer et al., 2017, De Cicco et al., 2020, Schalko et al., 2020). Furthermore, such accumulations have been shown to significantly modulate local scour depth around the pier, depending on the volume and porosity of the accumulated wood (Schalko et al., 2019a).

However, a critical and less-studied aspect in laboratory settings is the role of the geometric arrangement of bridge components. Recent studies highlight that the distance between a pier and an abutment is a pivotal control on flow contraction, energy loss, and backwater rise (Soori and Karami, 2024). Extending this, research has shown that this pier-to-abutment distance also significantly governs LW accumulation patterns and associated local scour, especially when considering realistic, porous wood accumulations rather than idealized debris shapes (Soori and Karami, 2025). Detailed turbulence analysis reveals that the strongest Reynolds shear stresses occur within the pier-abutment gap (Soori et al., 2025), and scour mechanisms for these configurations are driven by coupled lateral flow deflection and downflow, intensifying

with reduced clearance (Soori and Karami, 2026).

Field investigations corroborate this move towards complexity. Evidence indicates that severe, infrastructure-threatening clogging often involves mixed-composition debris (including anthropogenic material) and is critically driven by specific geometric factors like narrow pier spacing and low deck clearance (Poppema et al., 2025). This aligns with field-based analyses showing that disturbance magnitude and wood recruitment processes lead to non-uniform LW distributions in river corridors, with jams forming at natural and engineered obstructions (Wohl et al., 2018). Innovative approaches, including GIS-based modeling for wood supply estimation (Steeb et al., 2023) and integrative physical modeling (Friedrich et al., 2022), are advancing our ability to manage these complex processes at the catchment scale.

A review of the literature indicates that several key gaps remain: (1) most studies have focused on isolated bridge elements such as single piers or bridge decks, while the coupled pier–abutment system, as an effective geometric unit, has received comparatively limited attention; (2) the effect of initial large wood release conditions (including release distance, lateral position, and orientation), together with the systematic identification and quantification of a worst-case scenario as a design-oriented parameter, has largely been overlooked; and (3) the influence of pier-to-abutment spacing on LW accumulation probability, in a coherent and quantified form that is directly usable for hazard assessment and design, has not yet been provided. To address these gaps, the present study adopts a two-step approach to quantify LW accumulation probability (AP) in pier–abutment systems. AP is examined as a function of three main factor groups: (1) approaching flow conditions; (2) bridge-system geometry, with emphasis on the relative pier-to-abutment spacing; and (3) initial release conditions (distance, position, and orientation) and intrinsic LW characteristics (length, diameter, shape, and transport regime). The overall objective is to first identify the worst-case release scenario and then evaluate the relative influence of the remaining key parameters within the framework of that critical scenario. The outcomes provide a design-oriented and quantitative basis for an initial estimate of LW AP and for assessing clogging risk in bridges with pier–abutment configurations.

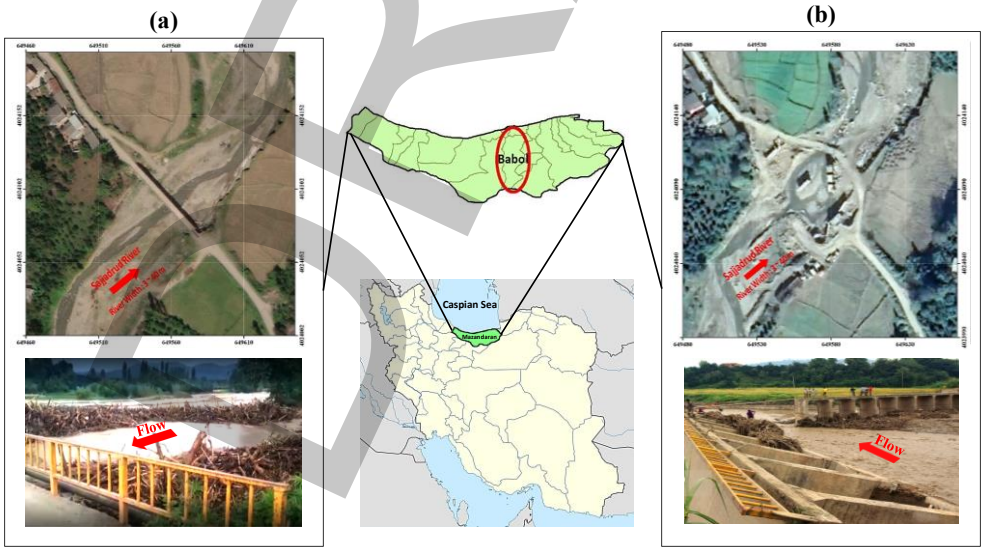

Fig. 1 Geographic location of Amir Deh bridge in Babol-Iran damaged due to flood and LW accumulation: (a) before the bridge destruction and (b) after the bridge destruction

2. Materials and Methods

2.1. Dimensional Analysis

Accumulation probability (AP) quantifies the likelihood that a single large wood (LW) element transported by the approach flow becomes trapped at a bridge obstruction. In the present study, AP is evaluated for the pier–abutment system. Accordingly, $p = 1$ denotes successful blockage at the obstruction, whereas $p = 0$ indicates free passage without trapping (Schmocker and Hager,

2011). The governing parameters used to express p are summarized in Equation (1).

$$p = \left(f_{Flow}(u_0, h_0, \rho_w, \sigma, g, v), \; f_{Structure}(B, L_a, D_p, x, G), \; f_{LW}(\rho_{LW}, L_{LW}, d_{LW}, x_{LW}, \theta_{LW}, PR_{LW}, Tr_{LW}) \right) \quad (1)$$

Here, u_0 is the approach flow velocity, h_0 is the normal flow depth, ρ_w is the water density, σ is the water surface tension, v is the kinematic viscosity, and g is the gravitational acceleration. The geometric parameters of the bridge and channel are: B, the channel width; L_a, the abutment length; D_p, the pier diameter; x, the distance between the bridge pier and the abutment; and G, the distance between adjacent bridge piers. Finally, the characteristics of the large wood element itself are defined by: its density (ρ_{LW}), length (L_{LW}), diameter (d_{LW}), the transverse release distance from the abutment nose to the flume centerline (x_{LW}), the orientation angle at release (θ_{LW}), the categorical release position (PR_{LW}: left bank L, centerline C, or right bank R), and its transport regime (Tr_{LW}).

Applying Buckingham Π theorem (Buckingham, 1914) and selecting ρ_w, u_0, and h_0 as repeating variables reduces Equation (1) to a set of dimensionless Π-terms, yielding the following relationship:

$$p = f(We, \mathrm{Re}, Fr_0, \rho_{LW}/\rho_W, x/L_{LW}, G/L_{LW}, d_{LW}/D_p, x_{LW}/B, \theta_{LW}, PR_{LW}, Tr_{LW}) \quad (2)$$

In Equation (2), the key dynamic similitude numbers are the Weber number ($We = {u_0}^2 h_0 \rho_{water}/\sigma$), the Reynolds number ($Re = u_0 h_0/v$), and the approach flow Froude number ($Fr_0 = u_0/gh_0$). The remaining terms are primarily geometric and material-related: ρ_{LW}/ρ_w is the relative LW density; x/L_{LW} and G/L_{LW} represent the relative pier–abutment distance and relative inter-pier spacing, respectively; d_{LW}/D_p is the relative LW diameter; and x_{LW}/B is the dimensionless upstream release distance. The orientation angle θ_{LW} (in radians), alongside the categorical variables PR_{LW} and Tr_{LW}, complete the set of governing dimensionless parameters.

For the specific experimental scope of pier–abutment interaction, Equation (2) was simplified based on three justified assumptions. Firstly, because the kinematic viscosity and surface tension were constant across all tests, the Weber number effect was considered negligible, and (We) was omitted (De Cicco, 2017, Schalko, 2018). Secondly, since the experiments were conducted under fully turbulent flow conditions, Reynolds number invariance was assumed, permitting the exclusion of (Re) (Wallerstein and Thorne, 1997, Bocchiola et al., 2008). Finally, with both water and LW densities held constant, the invariant density ratio ρ_{LW}/ρ_w was also removed.

Consequently, the simplified dimensional analysis leads to the final working dimensionless relationship:

$$p = f(Fr_0, x/L_{LW}, G/L_{LW}, d_{LW}/D_p, x_{LW}/B, \theta_{LW}, PR_{LW}, Tr_{LW}) \quad (3)$$

Equation (3) explicitly links the accumulation probability to the governing flow condition (Fr_0), key geometric ratios of the bridge (x/L_{LW}, G/L_{LW}, d_{LW}/D_p), and the characteristics of the incoming LW element. To evaluate the relative influence of these dimensionless parameters, a comprehensive experimental program was designed and executed. All tests were conducted under fixed-bed conditions in a rectangular flume at the Hydraulic Laboratory of Semnan University, Iran. The subsequent analysis of the resulting dataset aims to quantify the predictive capacity of Equation (3) for LW accumulation around bridge piers and abutments. A detailed account of the experimental configuration and methodology is provided in the Materials and Methods section.

2.2. Hydraulic Model

Physical flume experiments were conducted in the Hydraulics Laboratory of Semnan University, Iran, utilizing a large rectangular flume with dimensions of 14 m in length, 1 m in width, and 0.8 m in depth.

The channel features a fixed bed, and its slope (S_0) can be manually adjusted from 0% to 10%. To ensure high-quality flow conditions, a 2-meter-long flow straightener was installed at the channel inlet to dampen pump-induced secondary flows and surface waves. The subsequent 12-meter section of the channel was designated as the working reach for all experimental tests. Flow discharge was regulated using a pump with a nominal capacity of 110 L/s, which achieved a maximum flow rate of 90 L/s (82% efficiency). The downstream tailgate was adjusted to control the flow depth and establish the desired uniform approach flow conditions (denoted by

subscript 'o' and representing a state without LW accumulation). These approach conditions are defined by the flow depth (h_0), velocity ($u_0 = Q_0/Bh_0$), and the approach-flow Froude number ($Fr_0 = u_0/\sqrt{gh_0}$), where Q_0 is the discharge, B is the channel width (1 m), and g is gravitational acceleration. The three specific flow scenarios implemented in this study are summarized in Table 1. A schematic of the experimental setup, including key notation, is provided in Figure 2.

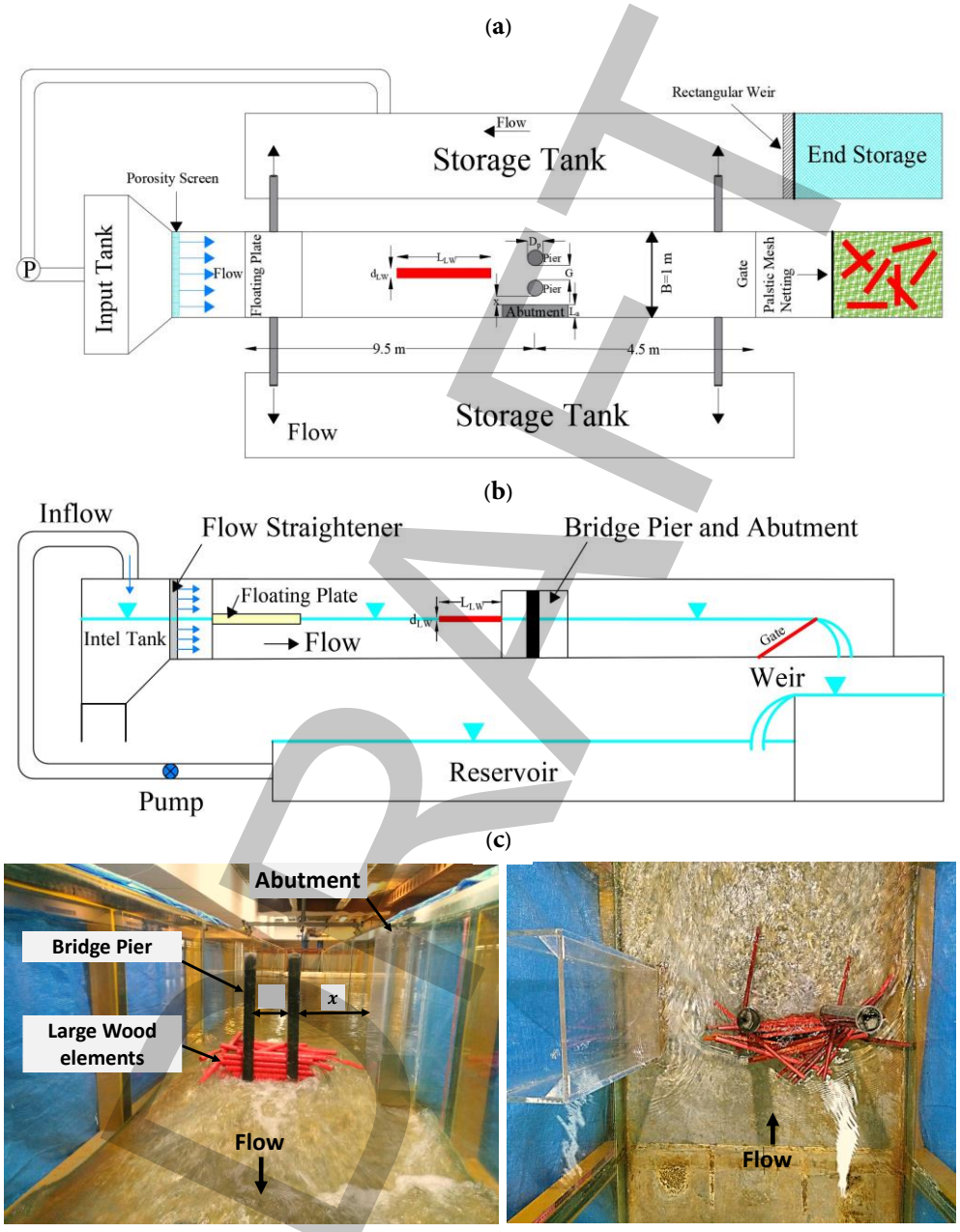

Fig. 2 Experimental set-up and notation for the LW accumulation probability tests: (a) plan view; (b) side view; and (c) example of LW accumulation over a fixed bed ($L_{LW} = 0.4\ m$, and $d_{LW} = 0.025\ m$)

Table 1- Summary of the three flow scenarios implemented in the experimental study

Scenario	Discharge (m^3/s)	Water depth (m)	Velocity (m/s)	Froude number (-)
1	0.016		0.16	0.16
2	0.026	0.1	0.26	0.26
3	0.036		0.36	0.36

Source: Authors' own work

2.3. Bridge Pier and Abutment Model

To examine the probability of LW accumulation, the experimental setup consisted of two cylindrical bridge piers ($D_p = 5\ cm$) and a rectangular abutment ($L_a = 15\ cm,\ B_a = 30\ cm$). The abutment geometry followed Dey and Barbhuiya (2005) and corresponded to a short vertical-wall abutment, satisfying $L_a/h_0 \leq 1$ and $B_a/L_a = 2$. The pier–abutment spacing (x) and inter-pier spacing (G) were selected based on the guidelines of Oben-Nyarko and Ettema (2011). Three spacing configurations, namely near, medium, and far, were considered (Table 2). For comparison across tests, x and G were subsequently expressed in dimensionless form and normalized by LW length, yielding the investigated ranges $0.75 < x/L_{LW} < 1.2$ and $0.38 < G/L_{LW} < 0.6$.

Table 2 Tested pier–abutment spacing configurations and corresponding dimensionless ratios

Position	$x(cm)$	$G(cm)$	$L_{LW}(cm)$	$x/L_{LW}\,(-)$	$G/L_{LW}\,(-)$
Near	7.5	15	25	0.30	0.60
			30	0.25	0.50
			35	0.21	0.43
			40	0.19	0.38
Medium	15	15	25	0.60	0.60
			30	0.50	0.50
			35	0.43	0.43
			40	0.38	0.38
Far	30	15	25	1.2	0.60
			30	1	0.50
			35	0.86	0.43
			40	0.75	0.38

Source: Authors' own work

2.4. Model Large Wood

Modeled LW elements consisted of natural wooden logs representing three morphological types: smooth cylindrical logs, branched logs, and needle wood. The cylindrical logs were geometrically scaled to lengths of $L_{LW} = 0.25, 0.3, 0.35$, and 0.40 m and diameters of $d_{LW} = 0.006, 0.012$, and 0.025 m (Figure 3 and Table 3). These dimensions were selected using a scale factor of $\lambda = 20$ based on field observations from the 2021 flood event in the Sajadrood River (Iran). The logs, primarily representing fir and cypress trunks (Braudrick and Grant, 2000, Bocchiola et al., 2008), had a uniform density of $\rho_{LW} = 625\ kg/m^3$, supporting hydrodynamic similarity under standard physical-modeling practice.

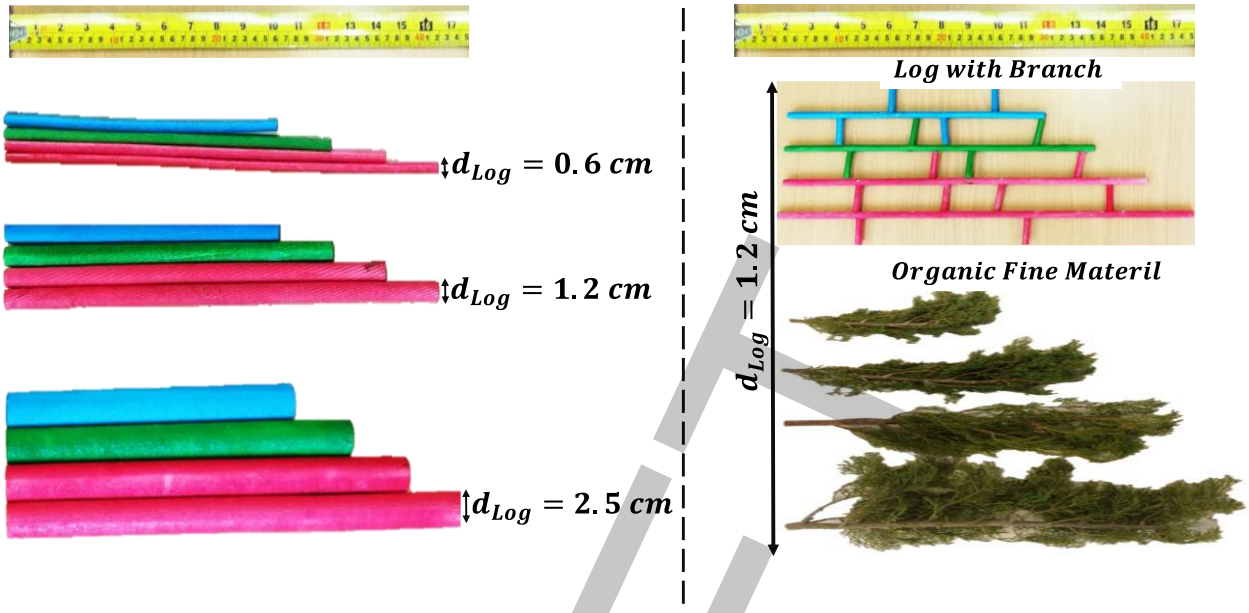

Fig. 3 Scaled large wood elements (L_{LW}, d_{LW}) and fine material used in the experiments $\lambda = 20$

Table 3 Geometric dimensions of the tested LW elements at prototype and model scales (scale factor $\lambda = 20$)

Code	Prototype Dimensions		Model-Scale Dimensions		
	$L_{LW}\ (m)$	$d_{LW}(m)$	$L_{LW}(m)$	$d_{LW}(m)$	L_{LW}/x
LW1	5	0.12, 0.24, 0.50	0.25	0.006	0.83
LW2	6		0.30	0.012	1
LW3	7, 8		0.35, 0.40	0.025	1.16, 1.33

Note: The prototype dimensions are based on field observations from the Sajjadrud River flood (2021) and were scaled down to the model using a linear scale factor of λ = 20.

2.5. Test program and procedure

A comprehensive experimental program was executed to quantify LW accumulation probability (p), structured around four primary test series (Table 4). The physical model consisted of two cylindrical piers and a rectangular abutment installed 9.45 m downstream of the flume inlet along the centerline to ensure fully developed approach flow. Pier-to-abutment spacing (x) and inter-pier spacing (G) were prescribed according to the test matrix (Table 4), with representative configurations including $x = 0.30\ m$ and $G = 0.15\ m$. Flow conditions were defined by a constant approach depth (h_0) of 0.10 m and three approach Froude numbers ($Fr_0 = 0.16, 0.26$, and 0.36), representing a range of common flood intensities. The LW release protocol was designed to isolate initial-condition effects. Individual logs were released from three lateral positions (left bank, centerline, and right bank), at three upstream distances from the abutment nose, and with three controlled orientation angles relative to the flow direction. For each configuration, p was evaluated by manually releasing 30 individual logs at a frequency of approximately one log every 10 s, defining an uncongested transport regime that minimizes log–log interactions and enables clear observation of capture mechanics. Each uncongested configuration was repeated 30 times to ensure statistical robustness. In addition, five replicate tests were conducted under a congested regime by releasing a bulk batch of 30 logs simultaneously. Methodological reproducibility is documented in Soori and Karami (2025). Post-processing computed p as the ratio of accumulated logs to the total number of released logs (De Cicco, 2017). Transported logs were intercepted by a downstream mesh net and

cleared regularly to prevent progressive backwater effects.

Table 4 Experimental parameters and variables used in test series A–D for LW AP

Series	Parameter Group	Variable	Symbol	Tested Values / Range
A	Repetitions	Number of Test Repetitions	N_{req}	200
B	Approach Flow Conditions	Froude number	Fr_0	0.1, 0.16, 0.26, 0.36, 0.46
		Flow depth	h_0	0.07, 0.10, 0.15, 0.20 (m)
		Flow velocity	u_0	0.08 - 0.46 (m/s)
C	Bridge Geometry	Number of Piers	n_P	1, 2
		Pier-to-Abutment Distance	x	7.5, 15, 30 cm
		Inter-Pier Spacing	G	15 cm
D	Large Wood (LW) Characteristics	Log Length	L_{LW}	25, 30, 35, 40 (cm)
		Log Diameter	d_{LW}	0.006, 0.012, 0.025 m
		Log Morphology (Shape)	Sh_{LW}	Smooth, branched, Needle-wood
		Transport Regime	T_{LW}	Uncongested, Congested
		Upstream Release Distance	x_{LW}	1, 3, 6 (m)
		Lateral Release Position	PR_{LW}	Left Bank, Centerline, Right Bank
		Initial Log Orientation	θ_{LW}	$0^{\circ}, 45^{\circ}, 90^{\circ}$

Note: Series A (Repetitions) refers to the total number of experimental runs conducted for statistical reliability. The specific values for parameters in Series B, C, and D represent the ranges over which the large wood accumulation probability was systematically investigated.

3. Results and Discussion

The experimental program followed a two-stage methodology. The first stage involved systematic scoping tests to identify the worst-case log placement scenario that maximizes accumulation probability. This scenario was defined by optimizing three initial conditions: lateral release position, longitudinal release distance from the abutment, and log orientation angle. Determining this critical baseline was necessary to standardize the subsequent core experiments. All following tests to quantify the effects of flow parameters, log properties, and bridge geometry were conducted under this consistent, worst-case initiation condition. This ensures the relative influence of each parameter is evaluated against a controlled and high-risk baseline.

3.1. Effect of LW release location on p

Figure 8 illustrates the effect of lateral release position (left bank, centerline, and right bank) on LW accumulation probability (p) as a function of Fr_0 for $L_{LW}/x = 0.83$ and 1.33. For both log lengths, the centerline release consistently produced the highest p, followed by the left bank and then the right bank, indicating strong path dependence and reduced trapping near the banks. Log length emerged as the primary control. For short logs ($L_{LW}/x = 0.83$) at $Fr_0 = 0.16$, p at the centerline was 0.45, whereas bank releases yielded 0.05 (left) and 0.023 (right). For long logs ($L_{LW}/x = 1.33$), centerline p decreased from 0.85 to 0.23 (73% reduction) as Fr_0 increased, reflecting reduced trapping under higher-flow-energy conditions. Overall, log length governs accumulation potential, while Fr_0 and release position modulate the response. These findings are consistent with Diehl (1997), who reported preferential mid-channel transport of wood in straight reaches.

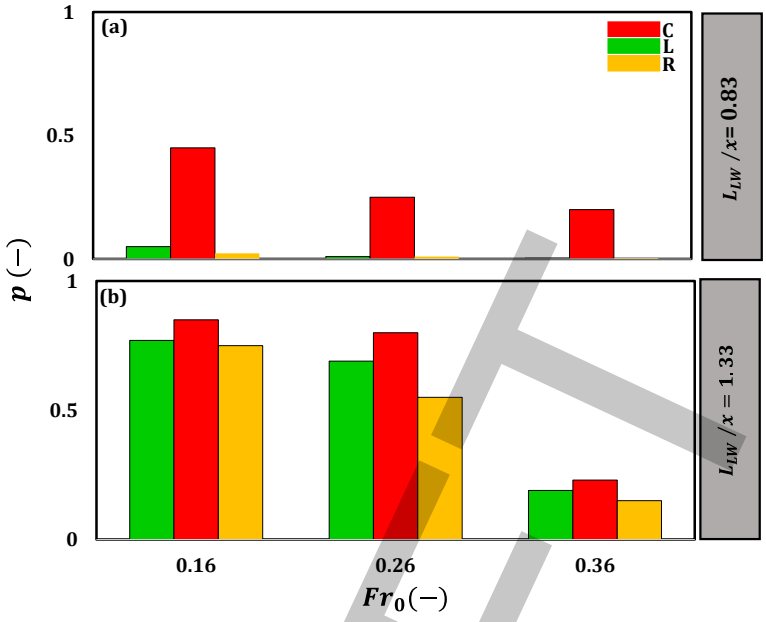

Fig. 4 p versus Fr_0 for LW release position (L, C, R) at $\theta_{LW} = \pi/2$ and $x_{LW}/B = 1$: (a) $L_{LW}/x = 0.83$ and (b) $L_{LW}/x = 1.33$

3.2. Effect of LW upstream release distance on p

Figure 5 shows LW accumulation probability (p) as a function of the approach-flow Froude number (Fr_0) for three normalized upstream release distances $x_{LW}/B = 1, 3, and\ 6$. Logs with $L_{LW}/x = 0.83$ and 1.33 were released along the channel centerline at a fixed worst-case orientation ($\theta_{LW} = \pi/2$). The results reveal a clear inverse dependence of p on release distance. For shorter logs ($L_{LW}/x = 0.83$) at $Fr_0 = 0.16$, p decreased from 45% at $x_{LW}/B = 1$ to 25% at $x_{LW}/B = 3$ and to 6% at $x_{LW}/B = 6$, corresponding to an overall 86% reduction. This confirms $x_{LW}/B = 1$ as the most critical (worst-case) release condition for initiating accumulations at the pier–abutment system. A similar decline was observed for longer logs ($L_{LW}/x = 1.33$), for which p decreased by 61% as x_{LW}/B increased from 1 to 6. Across both log lengths and all release distances, p also decreased systematically with increasing Fr_0.

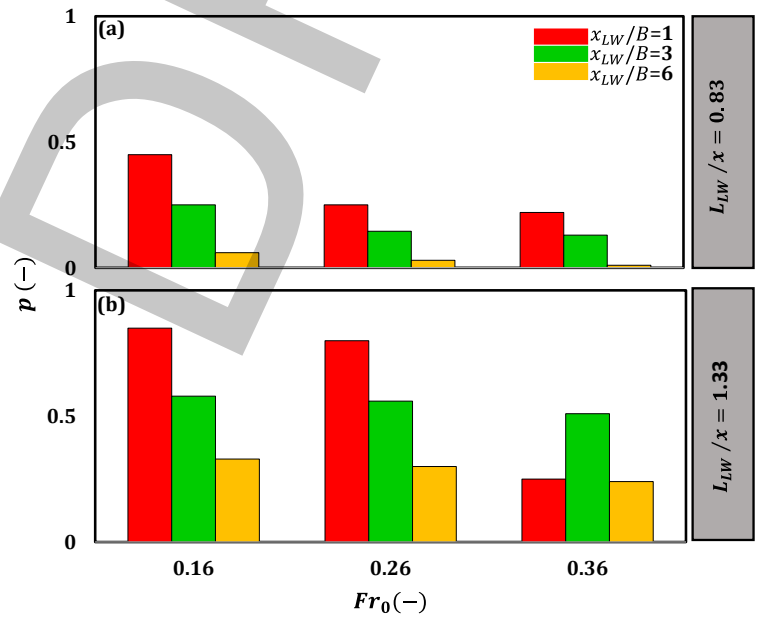

Fig. 5 p versus Fr_0 for different normalized release distances from the upstream abutment nose along the centerline, with $\theta_{LW} = \pi/2$: (a) $L_{LW}/x = 0.83$ and (b) $L_{LW}/x = 1.33$

3.3. Effect of LW orientation angle on p

Figure 6 illustrates the influence of initial log orientation on LW accumulation probability (p) as a function of the approach-flow Froude number (Fr_0). To represent a worst-case release configuration, logs with $L_{LW}/x = 0.83$ and 1.33 were released along the flume centerline at $x_{LW}/B = 1$ (i.e., 1 m upstream of the abutment nose) with three orientation angles: $\theta_{LW} = 0$ (parallel), $\theta_{LW} = \pi/4$, and $\theta_{LW} = \pi/2$ (perpendicular) to the flow. Observations indicate that logs released parallel to the flow ($\theta_{LW} = 0$) were typically advected downstream with limited interaction with the structure. With increasing orientation angle, the projected area normal to the flow increases, leading to greater hydrodynamic loading and a systematic increase in p. For $L_{LW}/x = 0.83$ at $Fr_0 = 0.16$, p increased from 12% at $\theta_{LW} = 0$ to 40% at $\theta_{LW} = \pi/4$, reaching 45% at $\theta_{LW} = \pi/2$. The same trend was more pronounced for longer logs ($L_{LW}/x = 1.33$), for which p reached 0.93 under the perpendicular orientation. Accordingly, a perpendicular initial alignment ($\theta_{LW} = \pi/2$) represents the most critical condition for LW accumulation at the pier–abutment system. These results are consistent with Davis (2001) and Schalko (2018), supporting the conclusion that perpendicularly oriented logs increase both accumulation probability and blockage potential.

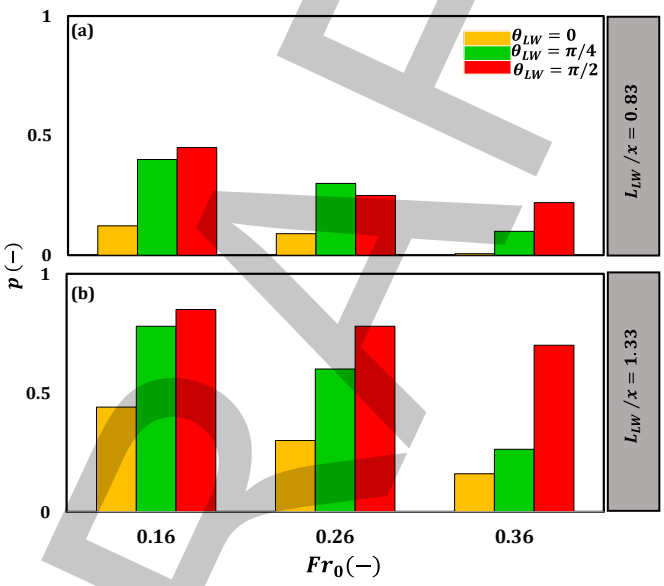

Fig. 6 p versus Fr_0 for different LW orientation angles at $x_{LW}/B = 1$ and centerline release: (a) $L_{LW}/x = 0.83$ and (b) $L_{LW}/x = 1.33$

Based on the systematic preparatory tests, the most critical configuration for LW accumulation was identified as centerline release at a normalized upstream distance of $x_{LW}/B = 1$ with a perpendicular orientation ($\theta_{LW} = \pi/2$).

3.4. Effect of Approach Flow Conditions on p

Figure 7 shows LW accumulation probability (p) as a function of the approach-flow Froude number (Fr_0) for a fixed log-length ratio ($L_{LW}/x = 0.83$) across flow depths $h_0 = 0.07 - 0.2\,m$. At $L_{LW}/x = 0.83$ and $h_0 = 0.1\,m$, p ranged from 0.06 to 0.60 over the tested Fr_0. For the shallowest flow ($h_0 = 0.07\,m$), p reached 0.71 at low Fr_0, but decreased to nearly zero as Fr_0 increased to 0.46. By contrast, for the largest depth ($h_0 = 0.2\,m$), p remained negligible (approx. 0%) across the full Fr_0 range, indicating that p decreases with increasing flow depth. These trends are consistent with previous studies (Lyn et al., 2003, Schalko et al., 2020) and support the inference that flow velocity, rather than flow depth or (Fr_0) alone, primarily governs accumulation probability. Nevertheless, (Fr_0) remains a key predictor of backwater rise, both in the presence of LW accumulations (Schalko et al., 2019b) and under unobstructed conditions (Soori and Karami, 2024).

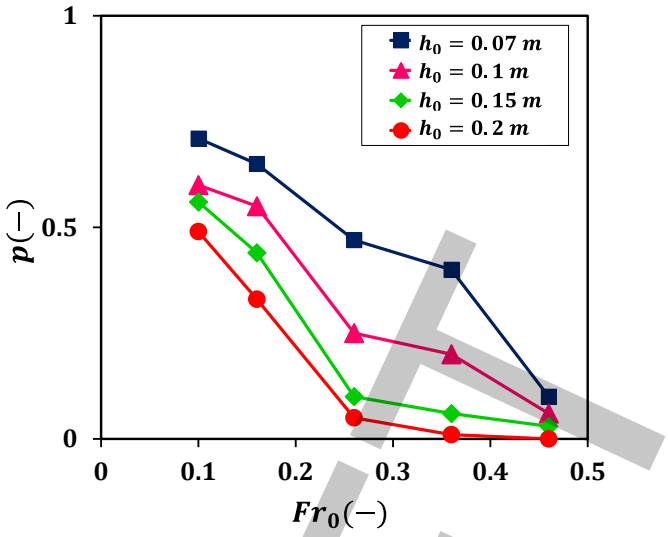

Fig. 7 p versus approach-flow Froude number (Fr_0) for different initial flow depths (h_0) at $L_{LW}/x = 0.83$

3.5. Effect of Large Wood Characteristics on p

Log length

Figure 8a shows p as a function of Fr_0 for $L_{LW}/x = 0.83, 1, 1.16$ and 1.33. At $Fr_0 = 0.16$, p equals 55% for $L_{LW}/x = 0.83$, 72% for $L_{LW}/x = 1$, 8% for $L_{LW}/x = 1.16$, and 87% for $L_{LW}/x = 1.33$, highlighting the strong influence of log length. In addition, p decreases with increasing Fr_0 for all tested L_{LW}/x, indicating that the approach-flow Froude number exerts a dominant control on p. These trends are consistent with previous studies (Schalko et al., 2020, De Cicco et al., 2020, Soori and Karami, 2025).

Log diameter

The effect of log diameter on accumulation probability was evaluated for relative diameters $d_{LW}/D_p = 0.12, 0.22$, and 0.5, at two log-length ratios $L_{LW}/x = 0.83$ and 1.33 (Figure 8b). For $L_{LW}/x = 0.83$ and a low Froude number ($Fr_0 = 0.16$), p increased substantially with diameter: $p = 22\%$ at $d_{LW}/D_p = 0.12$, $p = 51\%$ at $d_{LW}/D_p = 0.22$, and $p = 55\%$ at $d_{LW}/D_p = 0.5$, confirming the significant influence of log diameter. Furthermore, p decreased consistently with increasing approach-flow velocity u_0 for both log-length ratios, demonstrating that flow velocity exerts a governing control on accumulation probability, a finding consistent with earlier studies by Braudrick and Grant (2000) and Ruiz-Villanueva et al. (2016). In summary, accumulation probability increases with greater log length and diameter but decreases with higher approach-flow velocity. Consequently, L_{LW}, d_{LW}, and Fr_0 emerge as the decisive parameters for predictive design equations.

Log shape

Figure 8c evaluates the effect of log morphology by comparing smooth cylindrical, branched, and coniferous (needle-wood) logs on accumulation probability (p) at a fixed relative length ($L_{LW}/x = 0.83$).

At $Fr_0 = 0.16$, branched logs showed markedly higher accumulation ($p = 89\%$) and coniferous logs reached ($p = 93\%$), whereas smooth logs achieved only $p = 29\%$. As flow intensity increased to ($Fr_0 = 0.36$), probabilities declined to $p = 69\%$ for branched logs, (p=71%) for coniferous logs, and $p = 20\%$ for smooth logs. Although smooth logs consistently exhibited the lowest (p), the relative influence of morphology on p weakened with increasing Fr_0. Accumulation structure also depended on log type and flow conditions. Smooth logs typically formed rectangular jams around the pier–abutment system; coniferous logs displayed a similar pattern at low velocities. Smooth logs occasionally developed a semi-conical pile around the second pier. In contrast, branched logs initially remained buoyant and did not form a distinct jam geometry; at higher velocities, interlocking increased, producing more organized, rectangular accumulations downstream of the structures, coincident with a

reduction in p. These differences are attributed to surface roughness and branching geometry, which modify hydrodynamic drag and promote inter-log entanglement. However, the irregular and inherently random distribution of natural branches introduces substantial variability, limiting the development of a universal, deterministic predictive relationship for branched-log accumulation.

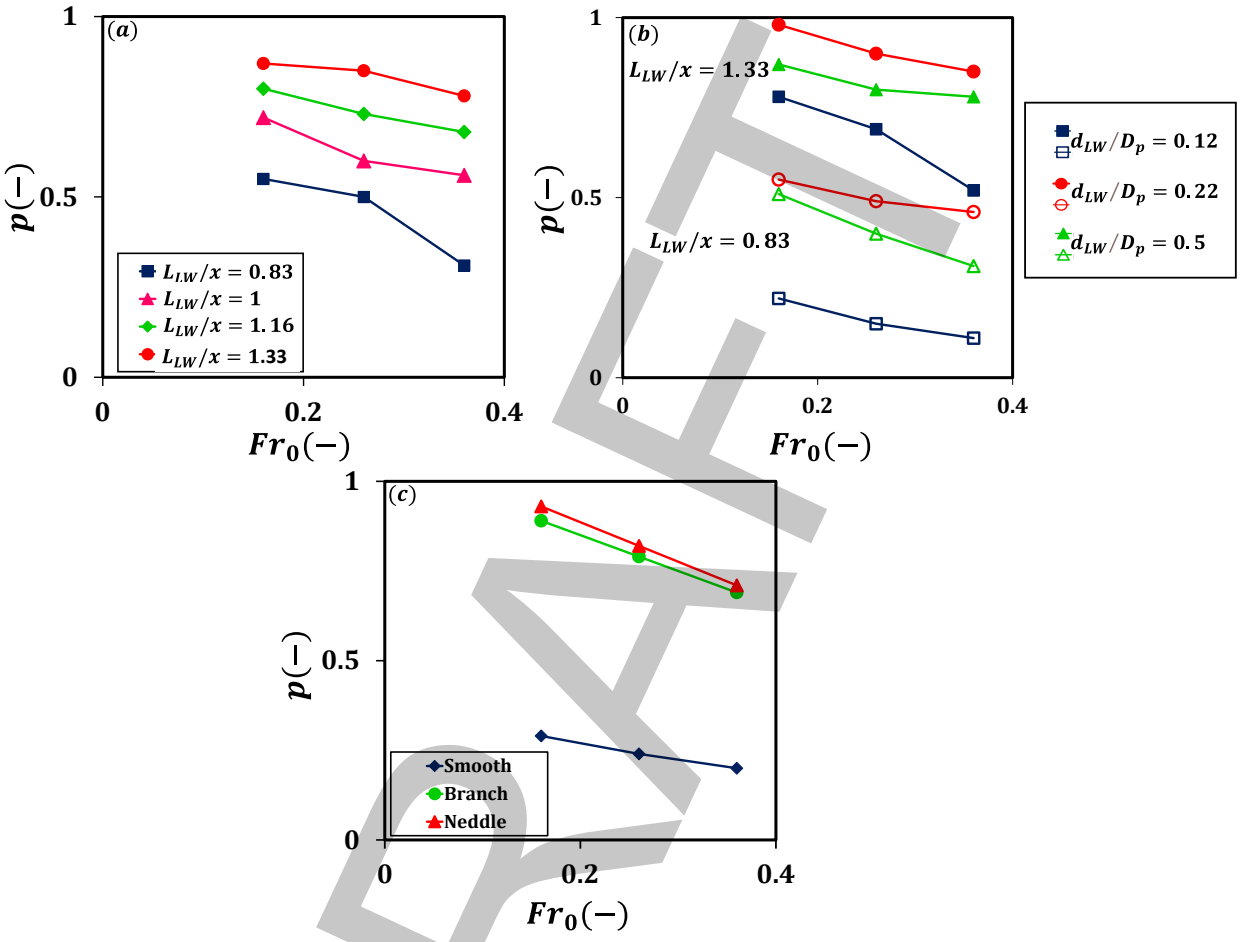

Fig. 8 p versus Fr_0 for: (a) different $L_{LW}/x = 0.83 - 1.33$ and $d_{LW}/D_p = 0.24$; (b) different d_{LW}/D_p with $L_{LW}/x = 0.83$ and 1.33; and (c) log-shape effects for $L_{LW}/x = 0.83$

3.6. Effect of Relative Distance Between Bridge Pier and Abutment on *p*

Figure 9 presents the physical model setup used to investigate LW accumulation over a fixed bed, spanning relative pier–abutment distances of $x/L_{LW} = 0.19 - 0.85$ for a single pier ($n_p = 1$). A log released along the flume centerline is advected downstream and typically undergoes slight rotation due to asymmetric hydrodynamic loading. As it approaches the pier, a torque develops because the downstream end enters a local low-velocity region in the pier wake while the upstream end remains in faster flow; this differential velocity enhances rotation and increases the likelihood of stable contact and trapping. The abutment further controls the approach path by deflecting the incoming flow toward the contraction zone and the pier, generating streamlines (visualized using potassium permanganate tracing) that steer the log into the pier–abutment interaction zone. The magnitude of this steering and the resulting trajectories depend on the approach velocity and x/L_{LW}: small spacings shorten the effective interaction zone and limit reorientation and interlocking, whereas larger spacings extend the interaction length, promoting rotation, engagement, and the formation of larger, more stable accumulations.

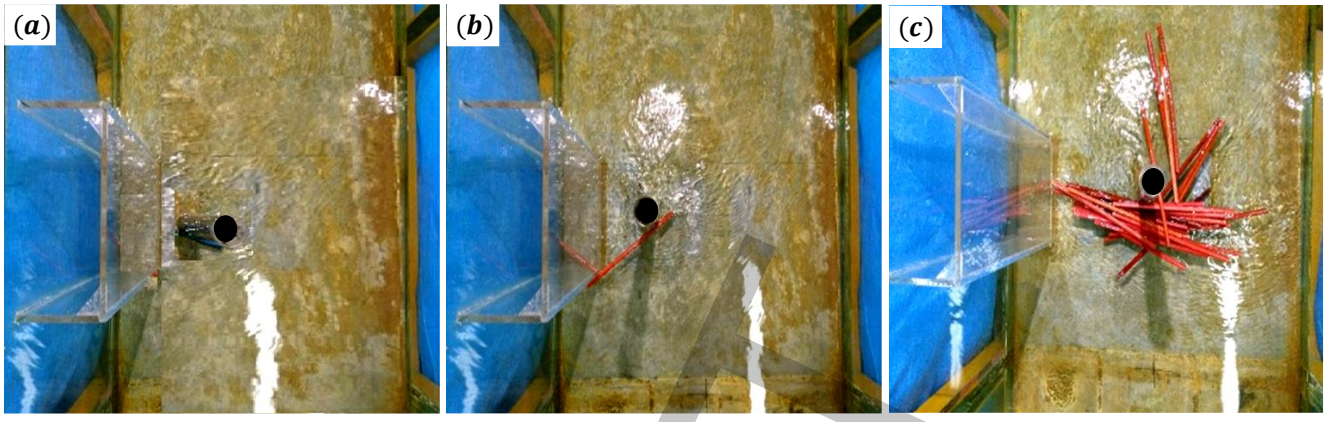

Fig. 9 Plan view of LW accumulation on a fixed bed for $L_{LW}/x = 1.33$, $d_{LW}/D_p = 0.24$, and $Fr_0 = 0.16$ (centerline release): (a) $x/L_{LW} = 0.19$, (b) $x/L_{LW} = 0.38$, and (c) $x/L_{LW} = 0.85$

Figures 10a and 10b illustrate the influence of the relative pier–abutment distance (x/L_{LW}) on accumulation probability (p) for uncongested LW transport at single pier and abutment. Results are reported for two normalized log-length ratios, $L_{LW}/x = 0.83$ and 1.33. For the shorter logs ($L_{LW}/x = 0.83$) under low-flow conditions ($Fr_0 = 0.16$), p increased markedly with increasing spacing: $p = 0$ at $x/L_{LW} = 0.3$, $p = 0.01$ at $x/L_{LW} = 0.6$, and $p = 0.18$ at $x/L_{LW} = 1.2$. This sensitivity was much stronger for longer logs ($L_{LW}/x = 1.33$), for which p increased by 0.78 across $x/L_{LW} = 0.19 - 0.85$, highlighting the dominant control exerted by relative spacing. Across all configurations, p decreased systematically with increasing approach Froude number. These results indicate that a pier located farther from the abutment ($x/L_{LW} = 0.85\ and\ 1.2$), and therefore more directly within the primary log-transport pathway, produces higher accumulation probabilities than a pier placed closer ($x/L_{LW} = 0.19\ and\ 0.3$), consistent with Diehl (1997) and Soori and Karami (2025). At the larger spacing, initial accumulations formed as an unstable network of interlocked elements. As the jam expanded and the flow intensified, the abutment-induced deflection shifted toward the pier, inducing rotational motion of the accumulated wood mass. This rotation promoted piece-by-piece detachment, with released logs transported downstream, thereby limiting further accumulation and producing the unstable "solid-phase" behavior described by Panici and de Almeida (2018).

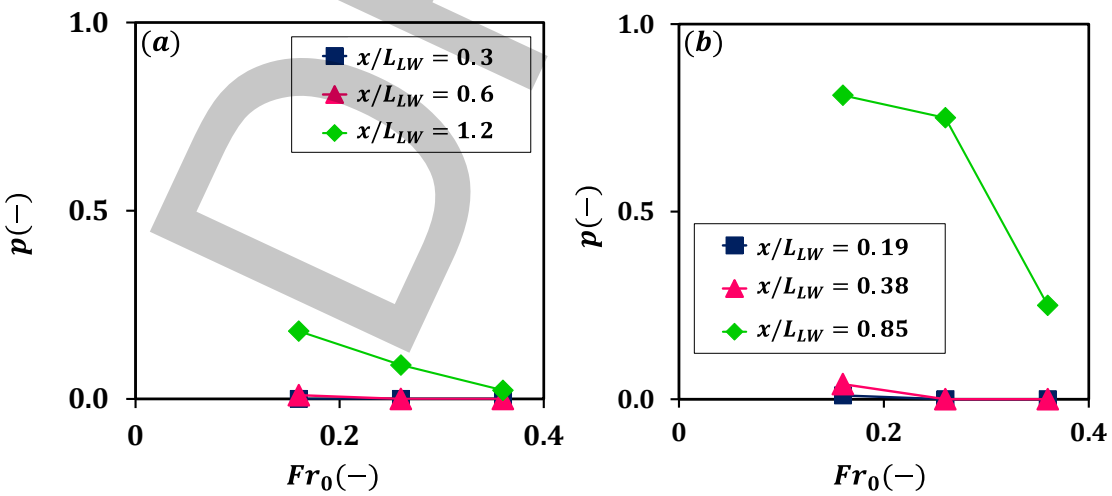

Fig. 10 p versus Fr_0 for different relative pier–abutment spacings (x/L_{LW}) with $n_p = 1$; (a) $x/L_{LW} = 0.3, 0.6, 1.2$ and (b) $x/L_{LW} = 0.19, 0.38, 0.85$

3.7. Effect of LW Transport Regime on p

The effect of LW transport regime on p is shown in Figure 11. The investigated regimes include uncongested and congested transport for logs with $L_{LW}/x = 0.83$ and 1.33. For $L_{LW}/x = 0.83$, p is on average 15.5% higher under congested transport than under uncongested conditions; this increase is most pronounced at lower Fr_0 and grows with the number of added logs. For $L_{LW}/x = 1.33$, congested transport yields an average increase of 82% in p relative to uncongested transport, and p again rises with the number of added logs. At $Fr_0 = 0.16$ under congested transport, p reaches a maximum of 100%. Moreover, for $L_{LW}/x = 1.33$, p remains $\geq 75\%$ for $Fr_0 < 0.36$, whereas for $L_{LW}/x = 0.83$ it is $p \leq 50\%$ under the same velocity range. Overall, the $L_{LW}/x = 1.33$ congested cases produce the highest accumulation probabilities observed in this study, with $p \geq 90\%$.

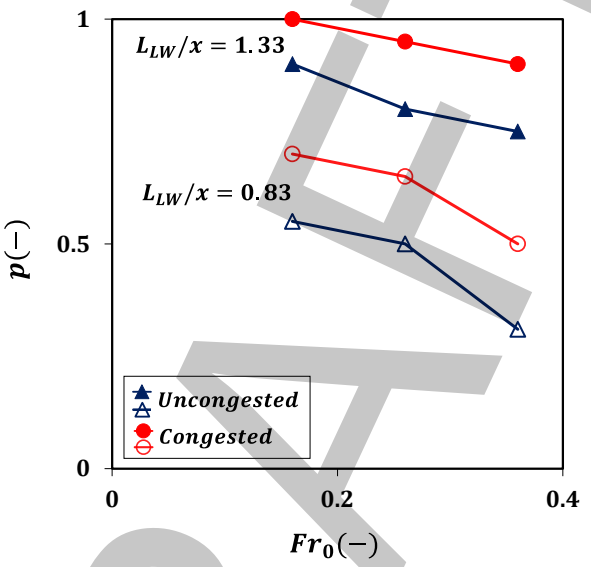

Fig. 11 p versus Fr_0 for uncongested versus congested LW transport at $L_{LW}/x = 0.83$ and 1.33

4. Conclusions and Outlook

Understanding woody-debris jams at bridge piers and abutments is essential for assessing bridge-failure and flood risks and for improving the design of future infrastructure. Accordingly, this study conducted flume experiments under log-length similitude at a scale factor of 20 to identify the worst-case accumulation scenario and the governing parameters controlling LW accumulation probability at pier–abutment systems. The practical objective is to provide a design-oriented basis for clogging-risk assessment and for optimizing controllable geometric features of pier–abutment configurations, rather than to control the initial placement of floating logs during floods. The key findings of this present study are:

1. Results for the worst-case LW accumulation scenario indicate that (i) centreline releases performed 1 m upstream of the abutment produced the highest accumulation probability, up to 86% greater than releases from 6 m upstream; and (ii) a perpendicular initial orientation ($\theta_{LW} = \pi/2$) maximized trapping, increasing accumulation probability by up to 375% relative to the parallel case.

2. LW accumulation probability (p) increases with increasing log length (L_{LW}) and diameter (d_{LW}), and it is further enhanced under congested transport conditions. Conversely, p decreases with increasing approach-flow velocity (u_0) and flow depth (h_0).

3. The experiments showed that LW accumulation probability increased with pier–abutment spacing, reaching its highest values at $x = 30\ cm$, where the piers were directly aligned with the main LW trajectory. This trend agrees with Diehl (1997) and (Soori and Karami, 2025), who reported that piers positioned within the log-transport path exhibit a higher trapping potential.

This work identifies practical design levers for mitigating LW accumulation, highlighting the importance of strategic planning in bridge design and maintenance. Specifically, optimizing pier–abutment spacing and reducing embankment lengths can substantially lower the probability of LW trapping. In addition, future work should combine these experimental findings with hydraulic and numerical modelling, while targeted field measurements could further clarify pier–log interactions and support evaluation of the proposed design relationships.

Acknowledgments

The authors gratefully acknowledge the financial support for this work that was provided by financial support by Iran National Science Foundation (INSF) [grant number: 99017275].

CRediT authorship contribution statement

S.S: Conceptualization; Methodology; Investigation; Data curation; Formal analysis; Visualization; Resources; Project administration; Supervision; Writing – original draft; Writing – review & editing; Manuscript development ; H.K: Validation, Resources.

5. References

BAGHERI-GAVKOSH, M., PANICI, D., PUTTOCK, A., DAUBEN, T. & BRAZIER, R. E. 2025. Hydrological Analysis and Impacts of Natural Flood Management Strategies: A Systematic Review. *Journal of Flood Risk Management,* 18**,** e70112.

BEZZOLA, G. R. & HEGG, C. 2007. Ereignisanalyse Hochwasser 2005, Teil 1– Prozesse, Schäden und erste Einordnung. *Umwelt-Wissen,* 707**,** 215.

BOCCHIOLA, D., RULLI, M. C. & ROSSO, R. 2008. A flume experiment on the formation of wood jams in rivers. *Water Resources Research,* 44.

BRADLEY, J., RICHARDS, D. & BAHNER, C. 2005. Debris control structures-evaluation and countermeasures: Hydraulic engineering circular 9. United States. Federal Highway Administration. Office of Bridge Technology.

BRAUDRICK, C. A. & GRANT, G. E. 2000. When do logs move in rivers? *Water resources research,* 36**,** 571-583.

BRAUDRICK, C. A., GRANT, G. E., ISHIKAWA, Y. & IKEDA, H. 1997. Dynamics of wood transport in streams: a flume experiment. *Earth Surface Processes and Landforms: The Journal of the British Geomorphological Group,* 22**,** 669-683.

BUCKINGHAM, E. 1914. On physically similar systems; illustrations of the use of dimensional equations. *Physical review,* 4**,** 345.

DAVIS, J. C. 2001. *Monitoring wilderness stream ecosystems*, US Department of Agriculture, Forest Service, Rocky Mountain Research Station.

DE CICCO, P. N. 2017. Experimental and numerical investigations on wood accumulation at bridge piers with different shapes.

DE CICCO, P. N., PARIS, E., SOLARI, L. & RUIZ-VILLANUEVA, V. 2020. Bridge pier shape influence on wood accumulation: Outcomes from flume experiments and numerical modelling. *Journal of Flood Risk Management,* 13**,** e12599.

DEY, S. & BARBHUIYA, A. K. 2005. Time variation of scour at abutments. *Journal of Hydraulic Engineering,* 131**,** 11-23.

DIEHL, T. H. 1997. Potential drift accumulation at bridges. *USGS. 95***,** 95.

FRIEDRICH, H., RAVAZZOLO, D., RUIZ-VILLANUEVA, V., SCHALKO, I., SPREITZER, G., TUNNICLIFFE, J. & WEITBRECHT, V. 2022. Physical modelling of large wood (LW) processes relevant for river management: Perspectives from New Zealand and Switzerland. *Earth Surface Processes and Landforms,* 47**,** 32-57.

GSCHNITZER, T., GEMS, B., MAZZORANA, B. & AUFLEGER, M. 2017. Towards a robust assessment of bridge clogging processes in flood risk management. *Geomorphology,* 279**,** 128-140.

GURNELL, A., PIÉGAY, H., SWANSON, F. & GREGORY, S. 2002. Large wood and fluvial processes. *Freshwater biology,* 47**,** 601-619.

KELLER, E. & SWANSON, F. 1979. Effects of large organic material on channel form and

fluvial processes. Earth Surface Processes, 4 (4), 361–380.

LAGASSE, P. F. 2010. *Effects of debris on bridge pier scour*, Transportation Research Board.

LYN, D. A., COOPER, T. J., YI, Y.-K., SINHA, R. N. & RAO, A. R. 2003. Debris accumulation at bridge crossings: laboratory and field studies.

OBEN-NYARKO, K. & ETTEMA, R. 2011. Pier and abutment scour interaction. *Journal of Hydraulic Engineering,* 137**,** 1598-1605.

PANICI, D. & DE ALMEIDA, G. A. 2018. Formation, growth, and failure of debris jams at bridge piers. *Water Resources Research,* 54**,** 6226-6241.

PANICI, D. & DE ALMEIDA, G. A. 2020. Influence of pier geometry and debris characteristics on wood debris accumulations at bridge piers. *Journal of Hydraulic Engineering,* 146**,** 04020041.

POPPEMA, D. W., BURGHARDT, L., BENET, L., WÜTHRICH, D., KLOPRIES, E. M., DEWALS, B. & ERPICUM, S. 2025. Bridge clogging in Belgium and Germany during the 2021 floods. *Water Resources Research,* 61**,** e2024WR039218.

RUIZ-VILLANUEVA, V., BADOUX, A., BOES, R., RICKENMANN, D., RICKLI, C., SCHALKO, I., SCHMOCKER, L., SCHWARZ, M., STEEB, N. & STOFFEL, M. Large wood research in Swiss watercourses. Proceedings of the International Conference on Fluvial Hydraulics, 2016. CRC Press Boca Raton, 2307-2314.

RUIZ-VILLANUEVA, V., MAZZORANA, B., BLADÉ, E., BÜRKLI, L., IRIBARREN-ANACONA, P., MAO, L., NAKAMURA, F., RAVAZZOLO, D., RICKENMANN, D. & SANZ-RAMOS, M. 2019. Characterization of wood-laden flows in rivers. *Earth Surface Processes and Landforms,* 44**,** 1694-1709.

SCHALKO, I. 2018. *Modeling hazards related to large wood in rivers.* ETH Zurich.

SCHALKO, I., LAGEDER, C., SCHMOCKER, L., WEITBRECHT, V. & BOES, R. 2019a. Laboratory flume experiments on the formation of spanwise large wood accumulations: Part II—Effect on local scour. *Water Resources Research,* 55**,** 4871-4885.

SCHALKO, I., LAGEDER, C., SCHMOCKER, L., WEITBRECHT, V. & BOES, R. M. 2019b. Laboratory flume experiments on the formation of spanwise large wood accumulations: I. Effect on backwater rise. *Water Resources Research,* 55**,** 4854-4870.

SCHALKO, I., SCHMOCKER, L., WEITBRECHT, V. & BOES, R. M. 2020. Laboratory study on wood accumulation probability at bridge piers. *Journal of Hydraulic Research,* 58**,** 566-581.

SCHMOCKER, L. & HAGER, W. H. 2011. Probability of drift blockage at bridge decks. *Journal of Hydraulic Engineering,* 137**,** 470-479.

SOORI, S., IKANI, N. & PU, J. H. 2025. Quadrant analysis of flow-structure interaction influenced by circular bridge piers around a rectangular abutment. *Ocean Engineering,* 341**,** 122688.

SOORI, S. & KARAMI, H. 2024. Laboratory study on relative energy loss and backwater rise at bridge piers and abutment. *Modeling Earth Systems and Environment,* 10**,** 1359-1373.

SOORI, S. & KARAMI, H. 2025. The Effect of Pier Placement on Large Wood Accumulation Probability and Local Scour at Bridge Piers and Abutments: Laboratory Flume Experiments. *Journal of Flood Risk Management,* 18**,** e70164.

SOORI, S. & KARAMI, H. 2026. Prediction and experimental verification of scour around complex bridge pier-abutment configurations using a validated FLOW-3D model. *Modeling Earth Systems and Environment,* 12**,** 54.

STEEB, N., RUIZ-VILLANUEVA, V., BADOUX, A., RICKLI, C., MINI, A., STOFFEL, M. & RICKENMANN, D. 2023. Geospatial modelling of large-wood supply to rivers: a state-of-the-art model comparison in Swiss mountain river catchments. *Earth Surface Dynamics,* 11**,** 487-509.

WALLERSTEIN, N. & THORNE, C. R. 1997. Impacts of woody debris on fluvial processes and channel morphology in stable and unstable streams.

WOHL, E., BLEDSOE, B. P., FAUSCH, K. D., KRAMER, N., BESTGEN, K. R. & GOOSEFF, M. N. 2016. Management of large wood in streams: an overview and proposed framework for hazard evaluation. *JAWRA Journal of the American Water Resources Association,* 52**,** 315-335.

WOHL, E., CADOL, D., PFEIFFER, A., JACKSON, K. & LAUREL, D. 2018. Distribution of large wood within river corridors in relation to flow regime in the semiarid western US. *Water Resources Research,* 54**,** 1890-1904.